Design Formulas for Flat Gradient Index Lenses with Planar or Spherical Output Wavefront

Hu, Weiya ; Martin, Caspar M. Coco; Cavallo, Daniele

DOI
10.1109/TAP.2024.3363433

Publication date
2024

Document Version
Final published version

Published in
IEEE Transactions on Antennas and Propagation

Design Formulas for Flat Gradient Index Lenses With Planar or Spherical Output Wavefront

Weiya Hu, Caspar M. Coco Martin, *Graduate Student Member, IEEE*, and Daniele Cavallo, *Senior Member, IEEE*

***Abstract*— A semi-analytical method is presented for the design of gradient index (GRIN) flat lenses. Closed-form expressions are derived to define the refractive index distribution of the lens, for several cases: collimating lenses with on-axis feed, collimating lenses with off-axis feed, lenses converting spherical wavefronts with different wavenumbers, lenses changing the focal number of a quasi-optical system, and Fresnel zone lenses. The design equations are validated by ray-tracing simulations in inhomogeneous media, implemented by numerical solution of the Eikonal equation.**

***Index Terms*— Geometrical optics (GOs), gradient index (GRIN) lenses, lens antennas, optical design, ray-tracing.**

I. Introduction

GRADIENT index (GRIN) lenses have been widely used as quasi-optical components in antenna systems. Presently, flat GRIN lens antennas are receiving particular attention because they provide high gain and quasi-optical beam steering capability. Such properties are beneficial for millimeter-wave (mmWave) communication and radar applications [1].

Compared with conventional homogeneous lenses, flat GRIN lenses can be more compact, low profile, and easy to integrate within planar antenna platforms. At mmWave and terahertz frequencies, the surface accuracy of curved lenses becomes a crucial parameter, while flat lenses can be realized with planar multilayer technology. Moreover, the inhomogeneous distribution of the refractive index can be used as additional degree of freedom to realize more flexible designs with desired output phase distribution.

The first step in the design of flat GRIN lenses is typically the evaluation of the refractive index distribution in each point of the lens. The obtained index profile can be subsequently implemented using, for example, 3-D-printed dielectric materials with different refractive indexes [2], or artificial dielectrics made of perforated dielectric slabs [3], or multiple layers of subwavelength metal periodic structure with variable spatial density [4], [5], [6].

Manuscript received 13 September 2023; revised 1 February 2024; accepted 4 February 2024. Date of publication 7 February 2024; date of current version 7 March 2024. *(Corresponding author: Daniele Cavallo.)*

The authors are with the Terahertz Sensing Group, Delft University of Technology, 2628 CD Delft, The Netherlands (e-mail: c.m.cocomartin@tudelft.nl; w.hu-11@student.tudelft.nl; d.cavallo@tudelft.nl).

Color versions of one or more figures in this article are available at https://doi.org/10.1109/TAP.2024.3363433.

Digital Object Identifier 10.1109/TAP.2024.3363433

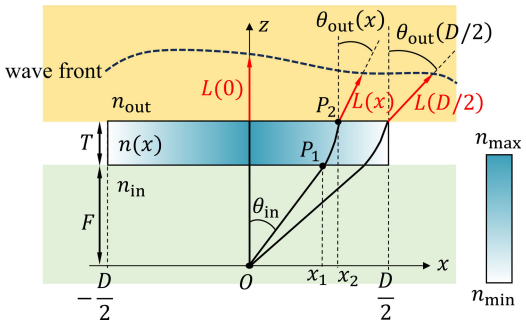

Fig. 1. Geometry of the flat lens.

Generally, there are different approaches to find the refractive index profile in a GRIN lens. A common method is based on transformation optics (TOs) [7], [8], [9], [10], [11], [12], [13]. To design a lens with certain properties, a specific coordinate transformation is applied that results in a corresponding map of the permittivity and permeability tensors [14], [15]. The resulting anisotropic materials can be difficult to realize in practice, thus often simplified electromagnetic parameters are selected. Another approach was proposed in [16] and uses field transformation (FT). This method is based on a discretization of the lens into unit cells, each with a certain unknown permittivity ε. The permittivity in each region can be found with a synthesis procedure that converts a given input field distribution into a desired output field distribution exiting the lens. Other GRIN lenses designs have been presented, based on combining ray-tracing solutions with optimization methods [17].

An alternative approach for designing GRIN lenses is to find analytical formulas based on geometrical optics (GOs) [6], [18], [19]. A similar approach is also used here. The goal of this article is to derive design formulas for GRIN flat lenses that are more general and can be applied to different planar and spherical transmitted wavefronts. We consider collimating lenses between two different media, with on-axis and off-axis feed, lenses converting spherical wavefronts with different wavenumbers, lenses changing the focal number of a quasi-optical system, and Fresnel zone lenses. The design equations are validated by ray-tracing simulations in inhomogeneous media.

II. Geometry of the Problem

Let us consider the general scenario in Fig. 1, where a lens with diameter D is illuminated by a point source placed at

focal distance F. The lens is located between two media with refractive indexes n_{in} and n_{out}, respectively. This assumption includes the case, for example, that the flat GRIN lens is used to illuminate a larger hyper-hemispherical lens with refractive index n_{out}, which is common for mmWave quasi-optical systems. For practical applicability, we assume that all the materials under analysis are nonmagnetic, thus only characterized by relative permittivity $\varepsilon_r \geq 1$ and relative permeability $\mu_r = 1$.

The permittivity distribution inside the lens is simplified to vary only in the radial direction, i.e., the refractive index for a 2-D cross section of the lens (xz-plane) is only a function of x and is constant with z inside the lens. An arbitrary ray with an incident angle θ_{in} propagates through the lens from $P_1 \equiv (x_1, F)$ to $P_2 \equiv (x_2, F+T)$ and enters the upper medium with transmitted angle θ_{out}.

A. Optical Path Length Equation

We assume that the distance between a generic point P_2, where the ray exits the lens, and a desired equi-phase surface is denoted as $L(x)$. The phase variations from the feed to this equi-phase wavefront for each ray should be equal to the one of the ray passing through the lens center

$$n_{\text{in}}F + n_{\max}T + n_{\text{out}}L(0) = \frac{n_{\text{in}}F}{\cos\theta_{\text{in}}} + \int_{P_1}^{P_2} n\,ds + n_{\text{out}}L(x). \tag{1}$$

A typical way to solve (1) requires imposing a condition for the edge of the lens, e.g., $L(D/2) = 0$ (the equi-phase front passes through the top edge of the lens) and $n(D/2) = n_{\min}$, which allows to solve for unknowns such as the thickness of the lens T or the maximum refractive index $n_{\max}$.

Closing the integral in the optical path is required for solving (1). The derivations are similar to the steps in [6] and are described in detail in Appendix. The main assumption is that the permittivity varies linearly between x_1 and x_2. The optical path can be related to the incident and transmit angles, to the thickness of the lens, and to the permittivity at the initial or final points

$$\int_{P_1}^{P_2} n\,ds = T\frac{\varepsilon_{r1} + S_1}{\sqrt{\varepsilon_{r1} - s_{\text{in}}^2}} = T\frac{\varepsilon_{r2} + S_2}{\sqrt{\varepsilon_{r2} - s_{\text{out}}^2}} \tag{2}$$

with

$$S_1 = \frac{-2s_{\text{in}}^3/3 - s_{\text{out}}^3/3 + s_{\text{in}}^2 s_{\text{out}}}{s_{\text{in}} - s_{\text{out}}} \tag{3}$$

$$S_2 = \frac{s_{\text{in}}^3/3 + 2s_{\text{out}}^3/3 - s_{\text{in}}s_{\text{out}}^2}{s_{\text{in}} - s_{\text{out}}} \tag{4}$$

where $s_{\text{in}} = n_{\text{in}}\sin\theta_{\text{in}}$, $s_{\text{out}} = n_{\text{out}}\sin\theta_{\text{out}}$, T is the thickness of the GRIN lens, and ε_{r1} and ε_{r2} refer to the relative permittivity at positions x_1 and x_2, respectively.

One can note that the solution depends on both s_{in} and s_{out}, which in turn are functions of θ_{in} and θ_{out}. Therefore, the design of the GRIN lens varies for different transmitted wavefront scenarios, which correspond to different θ_{out}. The general formulas reported here are applied in Sections III–IV to specific lens configurations.

B. Relationship Between Incident and Transmitted Angles

To solve the problem for different cases, it is also useful to derive a general relationship between θ_{in} and θ_{out}. From (44) and (48) in Appendix, we can write the following equality:

$$\frac{2}{T}\sqrt{\varepsilon_{r2} - s_{\text{out}}^2} = \frac{s_{\text{in}} + s_{\text{out}}}{x_2 - x_1}. \tag{5}$$

Since x_1 can also be written in terms of θ_{in} as $x_1 = F\tan\theta_{\text{in}}$, (5) can be solved for $\sin\theta_{\text{in}} = X$. After some algebraic manipulations, a quartic equation for X can be found as

$$B^2X^4 - 2ABX^3 + \left(A^2 + F^2 - B^2\right)X^2 + 2ABX - A^2 = 0 \tag{6}$$

with

$$A = x_2 - \frac{Ts_{\text{out}}}{2\sqrt{\varepsilon_{r2} - s_{\text{out}}^2}}, \quad B = \frac{Tn_{\text{in}}}{2\sqrt{\varepsilon_{r2} - s_{\text{out}}^2}}. \tag{7}$$

Equation (6) can be solved for X with standard methods to find the roots of polynomials. By discarding the complex solutions and limiting the range of the solutions to the appropriate range of angles (depending on the specific geometry), only one physical solution is retrieved.

C. General Expression of the Permittivity Distribution

The general expression of the permittivity profile in the lens can be found from (1) by defining

$$\Delta = n_{\text{in}}F + n_{\max}T + n_{\text{out}}L(0) - n_{\text{in}}\frac{F}{\cos\theta_{\text{in}}} - n_{\text{out}}L(x) \tag{8}$$

and using (2). Solving for the permittivity gives

$$\varepsilon_{r1}(x) = \frac{\Delta^2 - 2S_1T^2 + \Delta\sqrt{\Delta^2 - 4S_1T^2 - 4s_{\text{in}}^2T^2}}{2T^2} \tag{9}$$

or

$$\varepsilon_{r2}(x) = \frac{\Delta^2 - 2S_2T^2 + \Delta\sqrt{\Delta^2 - 4S_2T^2 - 4s_{\text{out}}^2T^2}}{2T^2} \tag{10}$$

where either (9) or (10) can be used, depending if the condition for the lens design is imposed on the input or output points of the rays through the lens. The general formulas derived in this section can now be applied to specific configurations.

III. Collimating Lens Design

The simplest scenario is the collimating lens, where the spherical wave emanating from the feed is converted into a planar wave exiting the lens, as shown in Fig. 2. The extra path term $L(x)$ on both sides of (1) vanishes, because the wave has the same phase everywhere when reaching the exit plane $z = T$. All the transmitted angles θ_{out} are equal to 0. Thus, (3) and (4) simplify as

$$S_1 = -\frac{2}{3}s_{\text{in}}^2, \quad S_2 = \frac{1}{3}s_{\text{in}}^2. \tag{11}$$

The terms in (1) depend on the lens thickness T, the incident angle θ_{in}, and the maximum refractive index $n_{\max}$ at positions

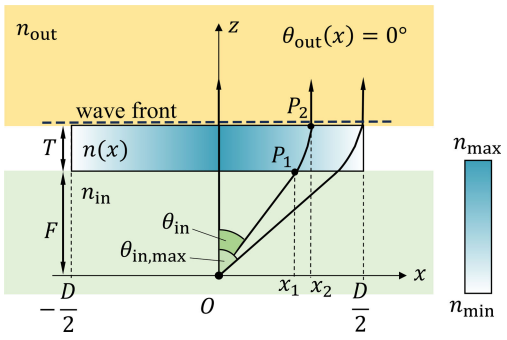

Fig. 2. Geometry for the collimating lens case.

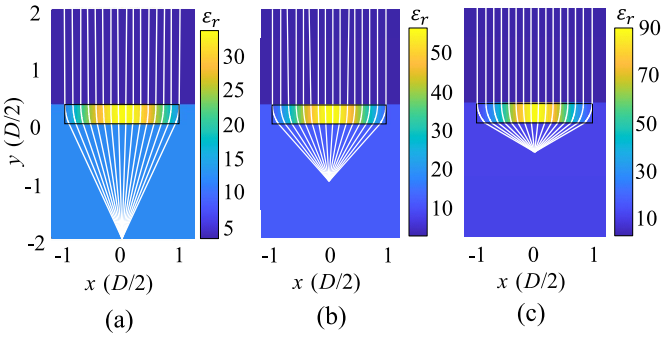

Fig. 3. Result of ray-tracing simulation for lenses placed between two media with refractive index $n_{in} = \sqrt{12}$ and $n_{out} = \sqrt{3}$, with different F/D ratios. (a) $F/D = 1$. (b) $F/D = 0.5$. (c) $F/D = 0.25$.

where the ray enters and exits the lens $x_{1/2}$. For collimating lenses that radiate to broadside, (1) can be rewritten as

$$n_{in}F + n_{max}T = \frac{n_{in}F}{\cos\theta_{in}} + \int_{P_1}^{P_2} nds \tag{12}$$

where the solution of the integral is defined in (2) as a function of θ_{in} and $\varepsilon_{r1/2}$.

To find the distribution of permittivity, we need to solve (12). In this equation, θ_{in} is known in each point and given by $\tan^{-1}(x_1/F)$, while $\varepsilon_{r1/2}$ are dependent variables. Therefore, the two unknowns of (12) are n_{max} and T. There are two possible options to design the lens, by either fixing n_{max} and finding T, or fixing T and finding the correspondent n_{max}. For example, in some designs one could opt to fix the thickness of the lens to a constrained value, resulting in a specific value of the maximum refractive index. Alternatively, one could constrain n_{max}, e.g., by the specific technology used to realize the lens, which results in a certain thickness.

Once the values of T and n_{max} are found, one can again apply (9) to find all the values of $\varepsilon_r(x)$ in any generic lens position x. The expression of Δ in (8) simplifies as follows:

$$\Delta = n_{in}F + n_{max}T - n_{in}\frac{F}{\cos\theta_{in}}. \tag{13}$$

A. Fixed n_{max}

With n_{max} as a given value, we apply (12) to the ray that impinges on the lens edge, corresponding to the maximum incident angle $\theta_{in,max} = \tan^{-1}[D/(2F)]$ and to the minimum permittivity $\varepsilon_{r1} = \varepsilon_{r,min}$

$$n_{in}F + n_{max}T = n_{in}\frac{F}{\cos\theta_{in,max}} + T\frac{\varepsilon_{r,min} - 2s_{in,max}^2/3}{\sqrt{\varepsilon_{r,min} - s_{in,max}^2}} \tag{14}$$

where $S_{in,max} = n_{in}\sin\theta_{in,max}$. The thickness of the lens can be found by inverting (14), resulting in

$$T = \frac{n_{in}F\left(\frac{1}{\cos\theta_{in,max}} - 1\right)}{n_{max} - \frac{\varepsilon_{r,min} - 2s_{in,max}^2/3}{\sqrt{\varepsilon_{r,min} - s_{in,max}}}}. \tag{15}$$

B. Fixed T

In Section III-A, the edge ray identified with the incident angle $\theta_{in,max}$ is intersecting the lens bottom surface at the edge $x_1 = D/2$. This ray is not bent as it propagates outside the lens. It is then convenient to consider as the last ray, the one exiting the lens at $x_2 = D/2$, rather than entering at the same x-position. Imposing the edge ray to exit at $x_2 = D/2$ typically improves the collimating performance of the lens at the edges. This assumption could not be used in the fixed n_{max} approach, because it would result in too many unknowns in (14). In the current approach, where the thickness is fixed, we can instead solve the problem assuming $x_2 = D/2$. However, with this assumption, $\theta_{in,max}$ becomes an unknown.

To find $\theta_{in,max}$, (5) and (6) can be solved for the ray passing through the upper edge: $x_2 = D/2$, $\varepsilon_{r2} = \varepsilon_{r,min}$, and the coefficients of the polynomial simplify as

$$A = \frac{D}{2}, \quad B = \frac{Tn_{in}}{2\sqrt{\varepsilon_{r2}}}. \tag{16}$$

By solving the quartic equation and discarding those non-physical roots (imposing that $\theta_{in,max}$ is a real angle, positive for $x > 0$ and negative for $x < 0$), the incident angle of the last ray can be found, and therefore, the total optical path length (OPL) through the lens edge can be accurately described. The refractive index at the center n_{max} can then be calculated based on (12) by substituting ε_{r2} with $\varepsilon_{r,min}$ and θ_{in} with $\theta_{in,max}$ as the root of the quartic equation.

C. Examples of Collimating Lens Design

The method is validated by applying ray-tracing simulations on the designed lens. The steps for ray-tracing simulations within the nonhomogeneous medium are introduced in [20] and [21]. The ray paths inside the nonhomogeneous lens can be computed with by solving numerically the system of ordinary differential equations deriving from the Eikonal equation [22], with the aid of MALTAB's built-in `ode45()` function.

With the design equations, considering $\varepsilon_{r,min} = \varepsilon_{r,in} = 12$, $\varepsilon_{r,out} = 3$, $D = 3\,\text{mm}$, $T = 0.17D$, three lenses with different F/D ratios were obtained. Fig. 3 shows the ray paths through these lenses computed using the ray-tracing simulations. The output rays are nearly parallel and vertical, with variations in the transmitted angles within $\pm 1°$, thus validating the proposed method.

As additional validation, a full-wave simulation of the first lens example with $F/D = 1$ is performed in CST. A 3-D

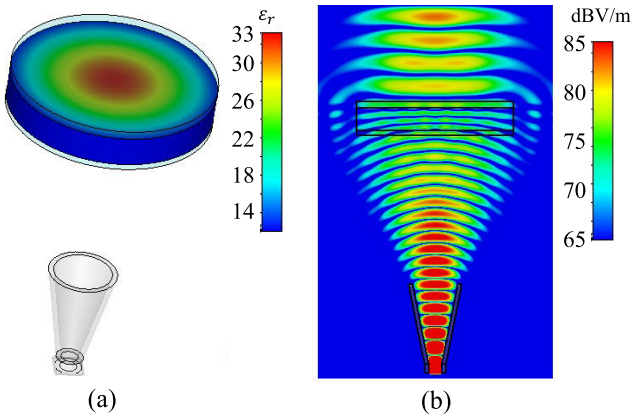

Fig. 4. (a) CST 3-D model of the lens example from Fig. 3 with a circular horn feed and (b) simulated electric field distribution on a cross section of the structure.

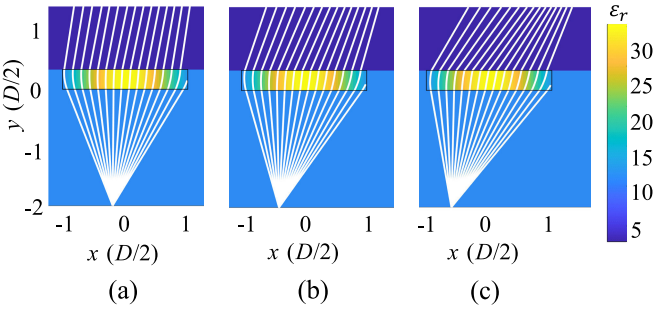

Fig. 5. Result of ray-tracing simulation for a lens with $F/D = 1$ placed between two media with refractive index $n_{\text{in}} = \sqrt{12}$ and $n_{\text{out}} = \sqrt{3}$, for different shift of the feed. (a) $\Delta_x = 0.1D$. (b) $\Delta_x = 0.2D$. (c) $\Delta_x = 0.3D$. The lens refractive index distribution is designed for broadside radiation.

model of the lens with a realistic circular horn feed is shown in Fig. 4(a). Matching layers of quarter wavelength at the calculation frequency are included to reduce reflections at the lens surfaces. The electric field distribution on a cross section of the structure is presented in Fig. 4(b). The corresponding aperture efficiency, calculated as the ratio of the simulated gain in CST to the maximum theoretical directivity from the lens aperture $(\pi D/\lambda)^2$, is 67%.

IV. Scanning Lens

It is possible to tilt the main beam of a dielectric lens antenna by shifting laterally the feed with respect to the lens axis. In Fig. 5, the results of the ray-tracing for the collimating lens with various feed shifts are shown, for a lens design for broadside radiation and $F/D = 1$. It can be noted that with the permittivity distribution designed for broadside maximum radiation, the GRIN lens scan performance is deteriorated. The phase and the direction of the transmitted rays undergo larger aberrations as the feed is shifted farther from the center.

Nevertheless, a flat lens that transforms the spherical beam into a planar beam pointing at θ_{scan} can be realized, with a procedure similar to the one described in Section III. For the scanning GRIN lens, shown in Fig. 6, $\theta_{\text{out}} = \theta_{\text{scan}}$ is valid across the lens, and $\theta_{\text{in}} = \tan^{-1}[(x_1 + \Delta x)/F]$ to account for the shift of the feed with respect to the lens axis.

Because in this case, the vertical ray impinging at the lens center is also bent inside the lens, it cannot be taken as the reference phase in the OPL equation. The OPL for an arbitrary

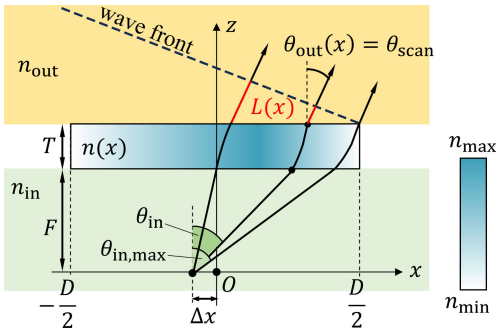

Fig. 6. Geometry for the scanning lens case.

position is then imposed to be equal to the ray passing through the lens edge

$$\frac{n_{\text{in}}F}{\cos\theta_{\text{in}}} + \int_{P_1}^{P_2} nds + n_{\text{out}}L(x) = \frac{n_{\text{in}}F}{\cos\theta_{\text{in,max}}} + \int_{P_{1\text{max}}}^{P_{2\text{max}}} nds \tag{17}$$

where $P_{1\text{max}} \equiv (F\tan\theta_{\text{in,max}}, F)$ and $P_{2\text{max}} \equiv (D/2, F+T)$ are the initial and end points of the ray through the lens edge, respectively. The integral on the right-hand side of (17) can be found with (2)–(4) by imposing $\varepsilon_r = \varepsilon_{r\text{min}}$, $\theta_{\text{in}} = \theta_{\text{in,max}}$, and $\theta_{\text{out}} = \theta_{\text{out,max}}$. The extra path $L(x)$ is given by

$$L(x) = \left(\frac{D}{2} - x_2\right)\sin\theta_{\text{scan}}. \tag{18}$$

The incident angle for the edge path $\theta_{\text{in,max}}$ is determined by solving (6), with

$$A = \frac{D}{2} + \Delta x - \frac{Ts_{\text{out}}}{2\sqrt{\varepsilon_{r,\text{min}} - s_{\text{out}}^2}}, \quad B = \frac{Tn_{\text{in}}}{2\sqrt{\varepsilon_{r,\text{min}} - s_{\text{out}}^2}}. \tag{19}$$

The OPL for other positions can be found by first writing x_2 from (5) as a function of incident angle θ_{in}

$$x_2 = T\frac{s_{\text{in}} + s_{\text{out}}}{2\sqrt{\varepsilon_{r1} - s_{\text{in}}^2}} + F\tan\theta_{\text{in}}. \tag{20}$$

Combining (2), (20) and substituting into (17), the OPL can be solved as in the previous case by defining Δ as

$$\Delta = \frac{n_{\text{in}}F}{\cos\theta_{\text{in,max}}} - \frac{n_{\text{in}}F}{\cos\theta_{\text{in}}} - n_{\text{out}}\left(\frac{D}{2} + \Delta x\right)\sin\theta_{\text{scan}} + \int_{P_{1\text{max}}}^{P_{2\text{max}}} nds + n_{\text{out}}F\tan\theta_{\text{in}}\sin\theta_{\text{scan}} \tag{21}$$

and replacing S_1 in (9) with

$$S_1' = S_1 - \frac{n_{\text{out}}}{2}(s_{\text{in}} + s_{\text{out}})\sin\theta_{\text{scan}}. \tag{22}$$

A. Examples of Lens Design

For comparison, the lenses redesigned to be optimized for scanning using the same specifications as the designed collimating lens $(F/D = 1)$ are simulated. The permittivity distributions and the ray-tracing simulation are presented in Fig. 7. The transmitted angles across the lenses are plotted in Fig. 8. It can be observed that now the transmitted angles

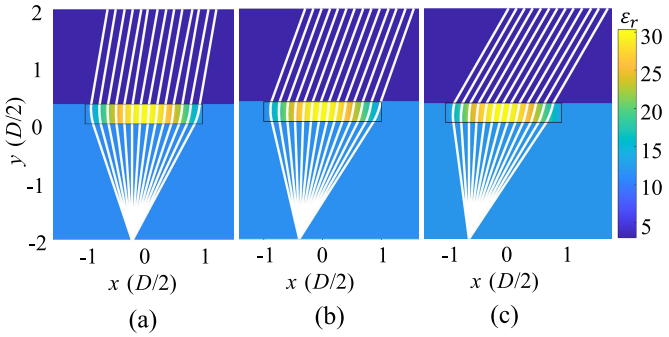

Fig. 7. Same as Fig. 5, but for refractive index distributions designed for each scan direction. (a) $\Delta x = 0.1D$, $\theta_{\text{scan}} = 10°$. (b) $\Delta x = 0.2D$, $\theta_{\text{scan}} = 20°$. (c) $\Delta x = 0.3D$, $\theta_{\text{scan}} = 30°$.

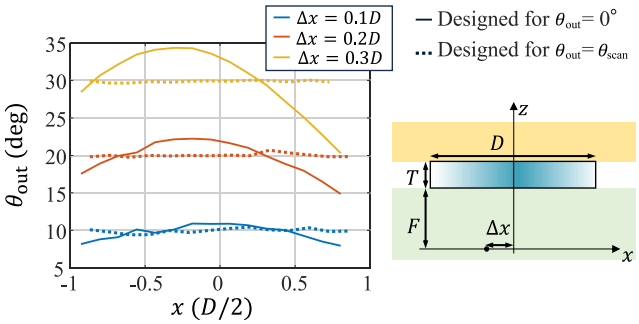

Fig. 8. Transmitted angle for feed shifting, comparing broadside and scanning design procedures.

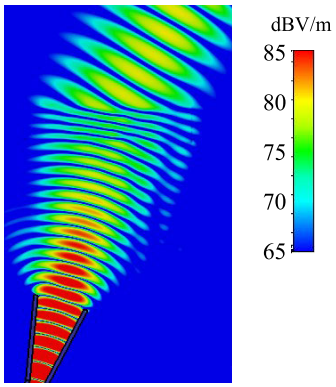

Fig. 9. Simulated electric field distribution on a cross section of the example in Fig. 7(c).

are constant, correcting for the aberration shown earlier when scanning with the lens designed for broadside radiation.

The simulated electric field distribution for the lens with $\Delta x = 0.3D$, computed by CST, is presented in Fig. 9. Also for this case, a circular horn is used as feed and tilted to point to the center of the lens. Matching layers of quarter wavelength at the calculation frequency are included. The transmitted wavefront is nearly planar and tilted by 30°, as by design.

V. Spherical Wavefront

In some cases, one can design the lens such that the output wavefront is not planar but still spherical, with the same or a different virtual focus. This example could be useful for application in which the flat lens is used as primary radiator

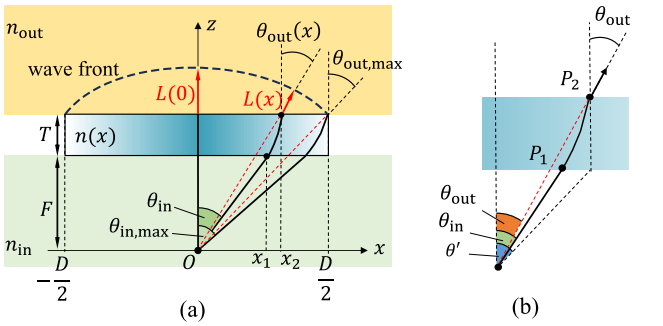

Fig. 10. (a) Geometry of spherical wavefront lens. (b) Definition of range for θ_{in}.

to illuminate a larger quasi-optical component, which might have a different F/D ratio.

A. Same Virtual Focus

In this case, the lens is located between two different media and is designed so that the spherical wavefront is maintained across the two media as if there was no medium discontinuity. In other words, the transmitted rays should appear as if they were emanating as straight rays from the same focal point [see Fig. 10(a)].

Since a spherical wavefront is desired on top of the lens, the function $L(x)$ in (1) is not zero across the lens. If a spherical wavefront intersecting the lens upper edge is considered, i.e., $L(D/2) = 0$, then $L(x)$ can be expressed as

$$L(x) = (F+T)\left(\frac{1}{\cos\theta_{\text{out,max}}} - \frac{1}{\cos\theta_{\text{out}}}\right) \tag{23}$$

where $\theta_{\text{out,max}}$ is defined as in Fig. 10(a), to be equal to

$$\theta_{\text{out,max}} = \tan^{-1}\left(\frac{D}{2(F+T)}\right). \tag{24}$$

The extra path from the lens to the wavefront for the central ray is equal to

$$L(0) = (F+T)\left(\frac{1}{\cos\theta_{\text{out,max}}} - 1\right). \tag{25}$$

Unlike the collimating case, the transmitted angle varies for each position and is an additional unknown of the problem, making the solution more complicate. Therefore, the mapping between each pair of $\theta_{\text{in}}, \theta_{\text{out}}$ must be found to solve (1).

For the sake of simplicity, we only consider here the simpler case where the lens thickness T is fixed while $n_{\max}$ is left as an open parameter of the design. From Fig. 10(a), we can also write

$$x_1 = F\tan\theta_{\text{in}}, \quad x_2 = (F+T)\tan\theta_{\text{out}}. \tag{26}$$

Similar to the steps described in the collimating case, $\theta_{\text{in,max}}$ can be found by solving the fourth order in (6) and (7).

By replacing $\theta_{\text{in}}, \theta_{\text{out}}, \varepsilon_{r2}$ with $\theta_{\text{in,max}}, \theta_{\text{out,max}}, \varepsilon_{r,\min}$ into (1), i.e., by considering the OPL for the edge ray at the right-hand side of (1), $n_{\max}$ can be found as

$$n_{\max} = \frac{1}{T}\left[n_{\text{in}}F\left(\frac{1}{\cos\theta_{\text{in,max}}} - 1\right) - n_{\text{out}}L(0) + \int_{P_{1\max}}^{P_{2\max}} n\,ds\right]. \tag{27}$$

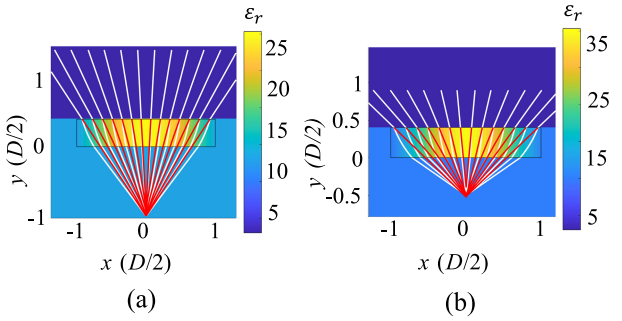

Fig. 11. Examples of lenses maintaining spherical wave across media. (a) $F/D = 0.5$. (b) $F/D = 0.25$.

With $n_{\max}$ known, to find the relative permittivity at any position on the lens with respect to each θ_{out}, the first step is to rewrite ε_{r2} in (5) as a function of incident angle θ_{in} using (26)

$$\varepsilon_{r2}(\theta_{\text{in}}) = s_{\text{out}}^2 + \frac{1}{4}\left[\frac{T(s_{\text{in}} + s_{\text{out}})}{(F+T)\tan\theta_{\text{out}} - F\tan\theta_{\text{in}}}\right]^2. \quad (28)$$

Unlike the collimating case, where $\theta_{\text{out}} = 0$ everywhere, θ_{out} is now a function that depends on the radial distance. To have the ray refocus on the focal point, the transmitted angle for the ray exiting lens at x_2 is given by

$$\theta_{\text{out}} = \tan^{-1}\left(\frac{x_2}{F+T}\right). \quad (29)$$

Because we are imposing θ_{out} to be given, the angle θ_{in} is not known. For every given value of x_2 and θ_{out}, θ_{in} can be found by sweeping the values of θ_{in} in a certain range and selecting the value that minimizes the difference between the left-hand side and the right-hand side of (1).

To avoid multiple solutions, the range is chosen as shown in Fig. 10(b): for a given θ_{out}, a single value of θ_{in} can be found when limiting the search in the range $(\theta_{\text{out}}, \theta')$, where $\theta' = \tan^{-1}(x_2/F)$. In this way, the mapping of θ_{in} and θ_{out} is found, and therefore ε_{r2} can be determined using (8) and (10) or from (28).

B. Examples of Lens Design

Two lenses with different F/D ratios are designed, based on the described procedure. Both the lenses radiate from silicon ($\varepsilon_r = 12$) to plastic ($\varepsilon_r = 3$) and have $\varepsilon_{r,\min} = 12$. The thickness of both the lenses is $0.2D$.

In Fig. 11, the white curves indicate the transmitted rays, while the red curves are the reverse extensions from the same rays toward the feed. It can be noted that most of the red curves converge in the focal point, which is the goal of this design.

The electric field distribution simulated with CST is shown in Fig. 12 for the example in Fig. 11(a). A circular horn that matches with F/D of 0.5 is used as feed. The transmitted wavefront from the plotted field distribution validates the lens design, since the virtual focus coincides with the phase center of the horn.

C. Spherical With Different Virtual Focus

In this section, a more general case of the spherical wavefront lens is studied, which considers a transmitted spherical

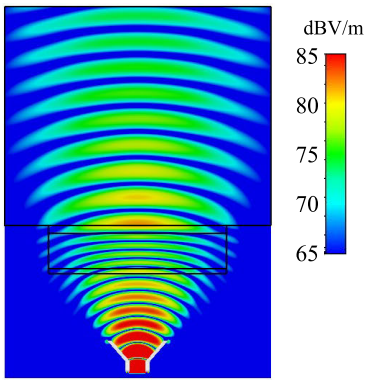

Fig. 12. Simulated electric field distribution on a cross section of the example in Fig. 11(a).

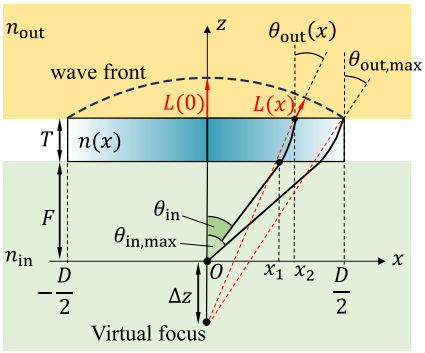

Fig. 13. Geometry of spherical wavefront lens with vertical displacement of the virtual focus.

wave with a different (virtual) focus. This is equivalent to a quasi-optical system that changes the F/D ratio. By doing this, it is possible to enlarge or narrow the equivalent subtended angle (from $\theta_{\text{in,max}}$ of the feed alone to $\theta_{\text{out,max}}$ of the feed combined with the GRIN lens), as shown in Fig. 13.

For example, the system could feed a larger elliptical or hyper-hemispherical lens. For mmWave and terahertz frequency, curved lenses are difficult to manufacture due to the required accuracy of the lens profile. The precision of the manufacturing is higher for shallow lenses, characterized by large F/D. Therefore, for the application with a secondary lens, the F-number of the system can be increased to simplify the manufacturing of the secondary lens.

Assuming now the distance between the virtual feed and the actual feed is Δz, the same steps in Section V-A can be followed, but replacing every occurrence of the term $(F+T)$ in (23)–(29) with the term $(F+\Delta z+T)$ that accounts for the new equivalent focal length.

The equations are applied to design lenses with $\varepsilon_{r,\min} = 12$ and radiating from silicon ($\varepsilon_r = 12$) to quartz ($\varepsilon_r = 3.8$). Fig. 14(a) shows the lens design for reducing the feed $\pm 48°$ illumination beam into a $\pm 20°$ beam. The thickness is $0.135D$. Δz of this case is calculated as $0.92D$. The corresponding F/D is increased from 0.45 to 1.37. Fig. 14(b) shows the lens with thickness $0.26D$, for shaping beams from $\pm 30°$ to $\pm 10°$, resulting in an F/D increasing from 0.87 to 2.58.

VI. Fresnel Zone Lens

As the last scenario, we consider a GRIN Fresnel lens. This is made by concentric zones, characterized by a 2π

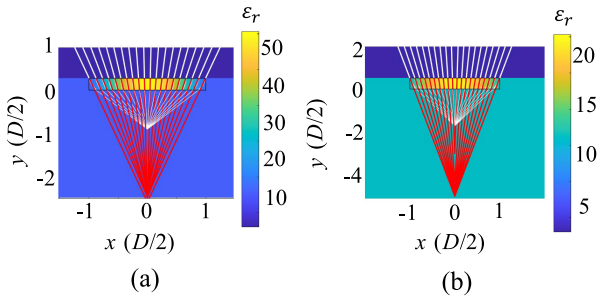

Fig. 14. Example of GRIN lenses for transforming focal ratio. Angular range from (a) ±48° to ±20° and (b) ±30° to ±10°.

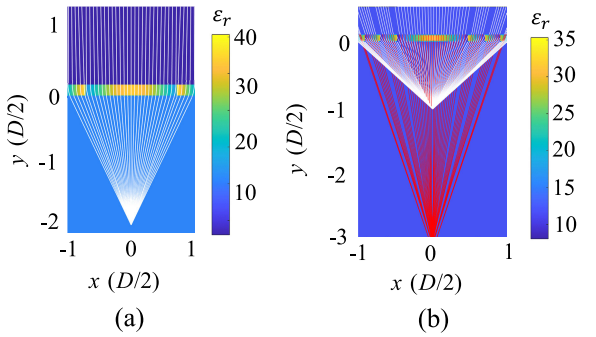

Fig. 15. Examples of GRIN Fresnel zone lenses. (a) Two-zone collimating lens with $\varepsilon_{r\min} = 12$, $n_{\text{in}} = \sqrt{12}$, $n_{\text{out}} = 1$, $T = 0.086D$, and $F/D = 1$. (b) Five-zone Fresnel lens with spherical wavefront conversion from ±48° to ±20°, with $\varepsilon_{r\min} = 12$, $n_{\text{in}} = \sqrt{12}$, $n_{\text{out}} = \sqrt{12}$, $T = 0.045D$, and $F/D = 0.45$.

phase wrapping at the transition between adjacent zones. This configuration can be used to reduce the thickness of the lens, at the cost of narrower bandwidth.

The different zones can be designed as individual flat GRIN lenses, by following the procedure described earlier. The only difference is that the OPL equation for the ith zone includes an extra term, coming from phase wrapping

$$n_{\text{in}}F + n_{\max}T + n_{\text{out}}L(0) = \frac{n_{\text{in}}F}{\cos\theta_{\text{in}}} + \int_{P_1}^{P_2} n\,ds + n_{\text{out}}L(x) - i\frac{2\pi}{k_0}. \quad (30)$$

where k_0 is the free-space wavenumber at the design frequency and i is equal to 0 for the center part increasing by 1 at each phase jump.

Here, we report in Fig. 15 two examples of Fresnel zone lens designs. In Fig. 15(a), a collimating lens is considered with two zones with $\varepsilon_{r\min} = 12$, $n_{\text{in}} = \sqrt{12}$, $n_{\text{out}} = 1$, and $T = 0.086D$, $F/D = 1$. In Fig. 15(b), a lens transforming a ±48° beam to a ±20° with five zones is considered. The lens is characterized by $\varepsilon_{r\min} = 12$, $n_{\text{in}} = \sqrt{12}$, $n_{\text{out}} = \sqrt{12}$, $T = 0.045D$, and $F/D = 0.45$.

It can be noted that the rays crossing the transition between zones are not plotted in Fig. 15. These rays undergo strong reflections due to the abrupt variation in permittivity at the interfaces between zones.

VII. Conclusion

Design equations for different type GRIN lenses were derived, to achieve transmitted wavefronts with arbitrary linear or quadratic phase profiles. The method provided is semi-analytical, based on closed-form expressions of the optical path through the GRIN lenses, and analytical or numerical solutions for all the lens parameters, to find the refractive index distribution.

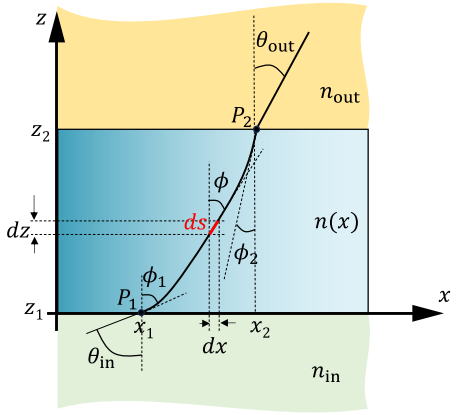

Fig. 16. Optical path inside the lens.

Different cases are studied, including collimating lenses with on-axis and off-axis feeds; lenses that transform spherical wavefronts across different media; lenses changing the focal number of a quasi-optical system; and Fresnel zone lenses.

Ray-tracing was used to validate the design procedure, confirming that the correct refractive index profile is obtained. Full-wave simulations of some of the examples with a realistic feed were also shown.

All the considered lens design examples were based on high relative permittivity values. Materials with such high permittivity can be practically implemented by means of artificial dielectric layers, which consist of periodic metal patches embedded in a host dielectric. A prototype flat lens based on artificial dielectrics is presented in a separate paper [23].

Appendix
Steps for Finding Optical Path Integration

The following derivations are based on the work of [6], but are extended for more general applicability to different GRIN lens designs. To find the distribution of permittivity across the lens, a closed-form expression for the optical path integration is needed. With reference to Fig. 16, considering a small section of arc ds on the ray's trajectory within the lens, according to the Pythagoras theorem, one can write

$$ds = \sqrt{dx^2 + dz^2} = \sqrt{1 + \left(\frac{dz}{dx}\right)^2}\,dx. \quad (31)$$

Therefore, the original integration along the arc can be transformed into the integration on x under the Cartesian coordinate system

$$\int_{P_1}^{P_2} n\,ds = \int_{x_1}^{x_2} n\sqrt{1 + \left(\frac{dz}{dx}\right)^2}\,dx. \quad (32)$$

It can be noted that inside the lens, since the refractive index only varies in a continuous manner along x, Snell's

law is verified at every vertical interface between infinitesimal slices. This can be expressed as

$$n(x)\cos\phi = \text{Constant} \tag{33}$$

which is valid for every position inside the lens, including both upper and lower boundaries. Therefore, the value of this constant can be found by applying (33) on the boundaries (at the points P_1 and P_2)

$$n_1\cos\phi_1 = n_2\cos\phi_2 \tag{34}$$

where n_1 and n_2 denote the refractive index at x_1 and x_2, respectively. Similarly, Snell's law can be applied on these positions for the horizontal interfaces

$$n_1\sin\phi_1 = n_{\text{in}}\sin\theta_{\text{in}} \tag{35a}$$

$$n_2\sin\phi_2 = n_{\text{out}}\sin\theta_{\text{out}}. \tag{35b}$$

Combining (33) and (35)

$$n_1^2\cos^2\phi_1 = n_1^2(1-\sin^2\phi_1) = \varepsilon_{r1} - n_{\text{in}}^2\sin^2\theta_{\text{in}} \tag{36a}$$

$$n_2^2\cos^2\phi_2 = n_2^2(1-\sin^2\phi_2) = \varepsilon_{r2} - n_{\text{out}}^2\sin^2\theta_{\text{out}}. \tag{36b}$$

From the trigonometric (33) can be written as

$$n\cos\phi = n\cot\phi\sin\phi = n\frac{\cot\phi}{\sqrt{1+\cot^2\phi}}. \tag{37}$$

The cotangent of the angle inside the lens can be related to the slope of the path by

$$\frac{dz}{dx} = \tan\left(\frac{\pi}{2}-\phi\right) = \cot\phi. \tag{38}$$

Thus, from (33), (34) and (38)

$$n\frac{\frac{dz}{dx}}{\sqrt{1+\left(\frac{dz}{dx}\right)^2}} = n_2\cos\phi_2. \tag{39}$$

By applying some algebraic steps, (39) can be rewritten as

$$\frac{dz}{dx} = \frac{n_2\cos\phi_2}{\sqrt{n^2-n_2^2\cos^2\phi_2}}. \tag{40}$$

Substituting (36b) and (40) into (32), we can write

$$\int_{P_1}^{P_2} n\,ds = \int_{x_1}^{x_2}\frac{n^2}{\sqrt{n^2-(\varepsilon_{r2}-n_{\text{out}}^2\sin^2\theta_{\text{out}})}}dx. \tag{41}$$

To close this integral, it is assumed that the relative permittivity changes linearly in the region between x_1 and x_2 with a slope a ($a>0$)

$$\varepsilon_r - \varepsilon_{r2} = a(x_2-x) \tag{42}$$

where a can be expressed as

$$a = \frac{\varepsilon_{r1}-\varepsilon_{r2}}{x_2-x_1}. \tag{43}$$

Using (36), a can also be expressed as

$$a = \frac{n_{\text{in}}^2\sin^2\theta_{\text{in}} - n_{\text{out}}^2\sin^2\theta_{\text{out}}}{x_2-x_1}. \tag{44}$$

(32) can be closed as follows:

$$\int_{x_1}^{x_2} n\,ds = 2\frac{s_{\text{in}}^3/3 + 2s_{\text{out}}^3/3 + (\varepsilon_{r2}-s_{\text{out}}^2)s_{\text{in}} - \varepsilon_{r2}s_{\text{out}}}{a} \tag{45}$$

where $s_{\text{in}} = n_{\text{in}}\sin\theta_{\text{in}}$, and $s_{\text{out}} = n_{\text{out}}\sin\theta_{\text{out}}$. Similarly, substituting (35a) and (36a) into (32), a dual expression of (45) as a function of ε_{r1} is obtained

$$\int_{x_1}^{x_2} n\,ds = 2\frac{-2s_{\text{in}}^3/3 - s_{\text{out}}^3/3 + (s_{\text{in}}^2-\varepsilon_{r1})s_{\text{out}} + \varepsilon_{r1}s_{\text{in}}}{a}. \tag{46}$$

The integration contains both a and ε_{r1} or ε_{r2} as unknowns. To solve this, another set of equations is needed. Supposing that the thickness of the GRIN lens is T, then the integration along the z-direction is

$$T = \int_0^T dz = \int_{x_1}^{x_2}\frac{dz}{dx}dx \overset{(40)}{=} \int_{x_1}^{x_2}\frac{n_2\cos\phi_2}{\sqrt{n^2-n_2^2\cos^2\phi_2}}dx. \tag{47}$$

This analytical integral expression can also be closed using commercial mathematics software and gives

$$T = \frac{2\sqrt{\varepsilon_{r2}-s_{\text{out}}^2}(s_{\text{in}}-s_{\text{out}})}{a}. \tag{48}$$

Similarly, if the equations with ε_{r1} are used, the dual expression for (48) is obtained

$$T = \frac{2\sqrt{\varepsilon_{r1}-s_{\text{in}}^2}(s_{\text{in}}-s_{\text{out}})}{a}. \tag{49}$$

Combining (45) with (48) and (46) with (49), the complete closed-form expression for the optical path inside the lens is found

$$\int_{P_1}^{P_2} n\,ds = T\frac{s_{\text{in}}^3/3 + 2s_{\text{out}}^3/3 + (\varepsilon_{r2}-s_{\text{out}}^2)s_{\text{in}} - \varepsilon_{r2}s_{\text{out}}}{\sqrt{\varepsilon_{r2}-s_{\text{out}}^2}(s_{\text{in}}-s_{\text{out}})} \tag{50a}$$

$$\int_{P_1}^{P_2} n\,ds = T\frac{-2s_{\text{in}}^3/3 - s_{\text{out}}^3/3 - (\varepsilon_{r1}-s_{\text{in}}^2)s_{\text{out}} + \varepsilon_{r1}s_{\text{in}}}{\sqrt{\varepsilon_{r1}-s_{\text{in}}^2}(s_{\text{in}}-s_{\text{out}})}. \tag{50b}$$

REFERENCES

[1] W. Hong et al., "Multibeam antenna technologies for 5G wireless communications," *IEEE Trans. Antennas Propag.*, vol. 65, no. 12, pp. 6231–6249, Dec. 2017.

[2] J.-M. Poyanco, F. Pizarro, and E. Rajo-Iglesias, "Cost-effective wideband dielectric planar lens antenna for millimeter wave applications," *Sci. Rep.*, vol. 12, no. 1, pp. 4204–4213, Mar. 2022.

[3] Y. He and G. V. Eleftheriades, "Matched, low-loss, and wideband graded-index flat lenses for millimeter-wave applications," *IEEE Trans. Antennas Propag.*, vol. 66, no. 3, pp. 1114–1123, Mar. 2018.

[4] Y. Su and Z. N. Chen, "A flat dual-polarized transformation-optics beamscanning Luneburg lens antenna using PCB-stacked gradient index metamaterials," *IEEE Trans. Antennas Propag.*, vol. 66, no. 10, pp. 5088–5097, Oct. 2018.

[5] A. Papathanasopoulos, Y. Rahmat-Samii, N. C. Garcia, and J. D. Chisum, "A novel collapsible flat-layered metamaterial gradient-refractive-index lens antenna," *IEEE Trans. Antennas Propag.*, vol. 68, no. 3, pp. 1312–1321, Mar. 2020.

[6] S. Zhang, R. K. Arya, W. G. Whittow, D. Cadman, R. Mittra, and J. C. Vardaxoglou, "Ultra-wideband flat metamaterial GRIN lenses assisted with additive manufacturing technique," *IEEE Trans. Antennas Propag.*, vol. 69, no. 7, pp. 3788–3799, Jul. 2021.

[7] A. Demetriadou and Y. Hao, "A grounded slim Luneburg lens antenna based on transformation electromagnetics," *IEEE Antennas Wireless Propag. Lett.*, vol. 10, pp. 1590–1593, 2011.

[8] C. Mateo-Segura, A. Dyke, H. Dyke, S. Haq, and Y. Hao, "Flat Luneburg lens via transformation optics for directive antenna applications," *IEEE Trans. Antennas Propag.*, vol. 62, no. 4, pp. 1945–1953, Apr. 2014.

[9] D. E. Brocker, J. P. Turpin, P. L. Werner, and D. H. Werner, "Optimization of gradient index lenses using quasi-conformal contour transformations," *IEEE Antennas Wireless Propag. Lett.*, vol. 13, pp. 1787–1791, 2014.
[10] O. Quevedo-Teruel et al., "Transformation optics for antennas: Why limit the bandwidth with metamaterials?" *Sci. Rep.*, vol. 3, no. 1, pp. 1–5, May 2013.
[11] A. M. Patel and A. Grbic, "Transformation electromagnetics devices based on printed-circuit tensor impedance surfaces," *IEEE Trans. Microw. Theory Techn.*, vol. 62, no. 5, pp. 1102–1111, May 2014.
[12] H. Eskandari and T. Tyc, "Controlling refractive index of transformation-optics devices via optical path rescaling," *Sci. Rep.*, vol. 9, no. 1, Dec. 2019, Art. no. 18412.
[13] Y. Su and Z. N. Chen, "A radial transformation-optics mapping for flat ultra-wide-angle dual-polarized stacked GRIN MTM Luneburg lens antenna," *IEEE Trans. Antennas Propag.*, vol. 67, no. 5, pp. 2961–2970, May 2019.
[14] H. Chen, C. T. Chan, and P. Sheng, "Transformation optics and metamaterials," *Nature Mater.*, vol. 9, no. 5, pp. 387–396, Apr. 2010.
[15] J. B. Pendry, A. Aubry, D. R. Smith, and S. A. Maier, "Transformation optics and subwavelength control of light," *Science*, vol. 337, no. 6094, pp. 549–552, Aug. 2012.
[16] S. Jain, M. Abdel-Mageed, and R. Mittra, "Flat-lens design using field transformation and its comparison with those based on transformation optics and ray optics," *IEEE Antennas Wireless Propag. Lett.*, vol. 12, pp. 777–780, 2013.
[17] J. Budhu and Y. Rahmat-Samii, "A novel and systematic approach to inhomogeneous dielectric lens design based on curved ray geometrical optics and particle swarm optimization," *IEEE Trans. Antennas Propag.*, vol. 67, no. 6, pp. 3657–3669, Jun. 2019.
[18] F. Maggiorelli, A. Paraskevopoulos, J. C. Vardaxoglou, M. Albani, and S. Maci, "Profile inversion and closed form formulation of compact GRIN lenses," *IEEE Open J. Antennas Propag.*, vol. 2, pp. 315–325, 2021.
[19] A. Paraskevopoulos, I. Gashi, M. Albani, and S. Maci, "Analytical formulas for refractive indices of a telescopic GRIN lens for aperture magnification," *IEEE Antennas Wireless Propag. Lett.*, vol. 21, no. 11, pp. 2206–2210, Nov. 2022.
[20] F. Maggiorelli, A. Paraskevopoulos, R. Giusto, M. Albani, and S. Maci, "Ray-tracing in dielectric inhomogeneous metalenses," in *Proc. 15th Eur. Conf. Antennas Propag. (EuCAP)*, Dusseldorf, Germany, Mar. 2021, pp. 1–5.
[21] D. Kulyabov, M. Gevorkyan, and A. Korolkova, "Software implementation of the Eikonal equation," in *Proc. Int. Conf (ITTMM)*, Moscow, Russia, Apr. 2018, pp. 25–32.
[22] M. Born and E. Wolf, *Principles of Optics*, 6th ed. Oxford, U.K.: Pergamon Press, 1980.
[23] C. M. C. Martin, W. Hu, and D. Cavallo, "Design of wideband flat artificial dielectric lenses at mmWave frequencies," *IEEE Trans. Antennas Propag.*, early access, Jan. 26, 2024, doi: 10.1109/TAP.2024.3357992.

Weiya Hu received the B.Sc. degree in electric and electronics engineering from the University of Electronics Science and Technology of China (UESTC), Chengdu, China, in 2017, and the M.Sc. degree (cum laude) in electrical engineering from the Delft University of Technology (TU Delft), Delft, The Netherlands, in 2023.

For his master thesis project, carried out in the Terahertz Sensing Group, TU Delft, he worked on design and measurements of artificial dielectric flat lenses.

Caspar M. Coco Martin (Graduate Student Member, IEEE) received the M.Sc. degree (cum laude) in electrical engineering from the Delft University of Technology (TU Delft), Delft, The Netherlands, in 2022. He is currently pursuing the Ph.D. degree with the Terahertz Sensing Group, TU Delft.

His research interests include wideband antenna arrays, artificial dielectrics, and analytical methods for electromagnetics.

Mr. Coco Martin was a recipient of the Excellent Presentation Award at the IEEE Ukrainian Microwave Conference in 2022.

Daniele Cavallo (Senior Member, IEEE) received the M.Sc. degree (summa cum laude) in telecommunication engineering from the University of Sannio, Benevento, Italy, in 2007, and the Ph.D. degree (cum laude) in electromagnetics from the Eindhoven University of Technology, Eindhoven, The Netherlands, in 2011.

From 2007 to 2011, he was with the Antenna Group, Netherlands Organization for Applied Scientific Research, The Hague, The Netherlands. From 2012 to 2015, he was Post-Doctoral Researcher with the Microelectronics Department, Delft University of Technology (TU Delft), Delft, The Netherlands. In 2015, he joined the Chalmers University of Technology, Gothenburg, Sweden, as a Visiting Researcher. He is currently an Associate Professor with the Terahertz Sensing Group, TU Delft. He has authored or coauthored about 180 papers published in peer-reviewed international journals and conference proceedings. His current research interests include analytical and numerical methods for antenna characterization, the design of antenna arrays, and on-chip antennas.

Dr. Cavallo is a Member of the European Association on Antennas and Propagation (EurAAP), the co-coordinator of the EurAAP working group "Active Array Antennas," and a Management Committee Member of the COST Action "Future communications with higher-symmetric engineered artificial materials (SyMat)." He was a recipient of the Best Innovative Paper Prize at the European Space Agency Antenna Workshop in 2008, the Best Paper Award in Electromagnetics and Antenna Theory at 11th European Conference on Antennas and Propagation (EuCAP) in 2017, and the 250 keuro "Veni" Personal Grant from the Netherlands Organization for Scientific Research in 2015. His students received the Best Student Paper Award at EuCAP 2013, the Special Mention at EuCAP 2015, the Else Kooi Prize in 2016, and the Honorable Mention at IEEE Antennas and Propagation Society International Symposium in 2019. He has served as an Associate Editor for IEEE TRANSACTIONS ON ANTENNAS AND PROPAGATION, from 2016 to 2022.